Wideband circularly polarized fractal antenna with SSRR metasurface for 5G applications

Original Scientific Paper

Maalim Al-Abbasi
University Malaya (UM),
Faculty of Engineering, Department of Electrical Engineering
Wilayah Persekutuan, Kuala Lumpur, Malaysia
maalim@siswa.um.edu.my

Tarik Abdul Latef
University Malaya (UM),
Faculty of Engineering, Department of Electrical Engineering
Wilayah Persekutuan, Kuala Lumpur, Malaysia
tariqlatef@um.edu.my

Abstract *–In this study, a 3.5 GHz wideband circularly polarised antenna design is presented. The suggested antenna is constructed using square and flower fractal shapes within the patch. The square fractal shapes and flower fractals are implemented inside the slot patch and in the top left and right corners of the patch. The key advantage of using this method is to increase the bandwidth of the antenna besides reduce the size and improve the axial ratio. Then a Square Split Ring Resonator (SSRR) metasurface is added above the antenna for enhancement of gain and back lobe. The metasurface is added on the front of the antenna in order to increase the gain directivity and decrease the sidelobes and back lobe. Using computer simulation software (CST), the proposed metasurface antenna is simulated and then constructed on FR4 substrate with dimensions of (ε_r=4.4 and h=1.6 mm). Operating bandwidth between 1.79 GHz and 5 GHz is achieved, the metasurface antenna's performance attained a fractional bandwidth of 91%. An improved gain of 3.05 dB is observed when metasurface is applied. A measured AR below 3 dB is achieved over the obtained bandwidth. The proposed fractal was reduced in size by 40.43% as compared to conventional antennas. The antenna recommended is suitable for use in the fifth generation (5G) applications.*

Keywords*: ircularly polarized, fractal antenna, metasurface, metamaterial, 5G, Axial ratio, bandwidth, CST software*

1. INTRODUCTION

The innovation of mobile and wireless communication applications toward fifth generation (5G) technology requires higher capacity and data rates compared to 4G technology [1-2]. For 5G mobile applications, a lower band of 3.5 GHz is recommended [3]. Antenna array networks were then suggested to increase the capacity and directivity of the proposed 5G mobile systems. Antennas can provide multiple beams with high gain and capacity toward the target. However, the antenna at this frequency (sub-6 GHz) is quite large and inflexible. At the suggested 5G bands, the critical design points for antennas are in terms of gain, size, backward radiation, sidelobes, and bandwidth. These terms are significantly important to providing a high-performance antenna for 5G bands. The alignment of the transmitter and receiver systems is necessary to reduce polarization mismatch losses when employing linearly polarized (LP) antennas in both transmission and reception systems. However, it is not required for a circularly polarized antenna (CP).

Typically, two orthogonal components of an electric field vector with equal amplitude are needed for circularly polarized antennas. This imposes a limitation on the bandwidth effectiveness of these antennas [4, 5]. On the other hand, axial ratio (AR) is a parameter that determines the polarization purity of CP. In this way, the perfect circular polarization, as seen at the poles of the Poincare sphere, The AR-enhanced circularly polarized antennas' bandwidth is increased using a variety of techniques. The first one is the radiator's built-in perturbation element [6]. Although it's a simple technique to produce circular polarization, it has a very narrow bandwidth. The second technique involves using a radiator with several feeds and external circuitry to create a phase shift between the feeds. This approach results in more wideband antennas, but their bulk is bigger, and their performance is constrained by the phase

shifter [6]. Wideband CP radiation can also be generated using crossed dipoles [7]. The stacked patch technique is another popular method for increasing the bandwidth and AR of CP microstrip antennas [8, 9-12].

It is also feasible to enhance the CP slot antenna's bandwidth by combining the CP slot antenna with a patch antenna. A circular slot antenna fed by a microstrip line with a parasitic patch antenna is presented in [10]. The inverted L-shaped feeding line achieves the CP radiation of the circular slot, similar to the CP slot antenna examined in [11]. The 3 dB AR bandwidth can be expanded to 45% when the parasitic patch is excited as well. This produces an additional CP resonance, which is then combined constructively with the CP resonances from the slot and the patch. The fundamental design of these CP patch antennas consists of the corners-truncated square patch [12], rectangular patch [13], elliptical patch [14], and slot- loaded square patch [15]. These fundamental CP patch antennas have a very small bandwidth, usually between 1% and 2%. CP patch antennas' bandwidth is increased using a variety of techniques, especially the AR bandwidth. However, aside from the size and complexity constraints, all of these designs still have restricted bandwidth and a 15% maximum AR improvement. Furthermore, the antenna designers typically used many radiators or complicated polarizers to feed radiators in circularly polarized microstrip antennas in order to achieve high gain, wide impedance bandwidth, wide axial ratio bandwidth, and beam width performance. As a result, the microstrip patch antenna's size increases and it is no longer appropriate for use with small, portable wireless devices. Metamaterials have therefore been suggested as a solution to these problems. According to definitions, metamaterials are artificial materials with special electromagnetic characteristics not found in natural materials [16]. On the other hand, metamaterial structures have demonstrated potential electromagnetic properties that are applicable to industry and microwave sub-6 GHz bands. Furthermore, a material that derives its properties from its structure rather than its composition directly is referred to as a metamaterial. Permittivity and permeability are the fundamental characteristics of metamaterials constructions [17]. Other properties such as refractive index, characteristic impedance, etc. can be defined by permittivity and permeability. Most natural materials exhibit a permeability equal to free space permeability $\mu 0$ and permittivity greater than the permittivity of free space $\varepsilon 0$ [18]. The goal of a metamaterial approach to antenna design is to improve antenna efficiency, bandwidth, weight, directivity, and other factors while overcome the limitations of conventional design techniques. It is well known that there is an inverse relationship between antenna size and radiation frequency. To reduce the size of an antenna while maintaining radiation efficiency, metamaterial structures are used to modify the dispersion relation or the near field characteristic of the antenna. [19, 20].

In response to the demands of portable communications devices, this paper presents a circularly polarized using a fractal antenna at 3.5 GHz with metasurface superstrate above the patch by using metamaterial structures implementation as superstrate placed on the top of the antenna patch with air gap distance with high performance. Recently metasurface antennas have been widely applied for increase gain and bandwidth enhancement for microstrip antenna due to the features of low profile, wide bandwidth, and easy implementation. Various metasurface antennas have been developed for compact size, wideband, low profile, or circular polarization applications [21-24]. Typically, a metasurface layer is built using an array of uniform periodic unit cells in various shapes, such square, rectangle, H-shaped, etc. After that, the metasurface is positioned above or below the main radiating element. [25].

This work contributes a new method to create a compact, high-gain, single-feed, single-layer microstrip antenna utilizing a fractal square array shaped with a modified slot ground to increase the return loss and avoid mismatching during fabrication and measurement process. When compared to previous procedures used on patches of a comparable size, this method is naturally simple and achieves a wideband axial ratio. The suggested antenna is designed to achieve a wideband of more than 2 GHz and an axial ratio of the same bandwidth. The antenna is created using the fractal square iteration technique. Then it is integrated into an array of fractal square iterations inside the patch. The suggested antenna is constructed from a FR-4 substrate with dimensions of (ε_r=4.4) and a height of h=1.6 mm. The antenna can be employed in future 5G applications because the measured findings were in good agreement with the simulated outcomes.

2. ANTENNA DESIGN WITH METASURFACE

This section focused on realizing a wideband circularly polarized fractal antenna with SSRR metamaterial as metasurface superstrate placed above the patch with high performance which can be used in the characterization of 5G base station.

2.1. FRACTAL ANTENNA DESIGN

The design of the fractal antenna with square iterations is realized in four steps as follows; firstly, the required formulas used to find the length and width of the patch are provided in [8].

Hence, when the frequency is resonated at 3.5 GHz with ε_r=4.4 and thickness of 1.6 mm, the square length (L_p) is about 27.4 mm. A cut is made inside the square patch in order to study the effects of the slot square on the return loss before inserting the fractal shape. Fig. 1 depicts the basic and slotted structure of the antenna. The layout of the antenna in Fig.1 has a key benefit of simplicity in modifying its structure. While fractal iteration shape could be easily applied on the antenna structure.

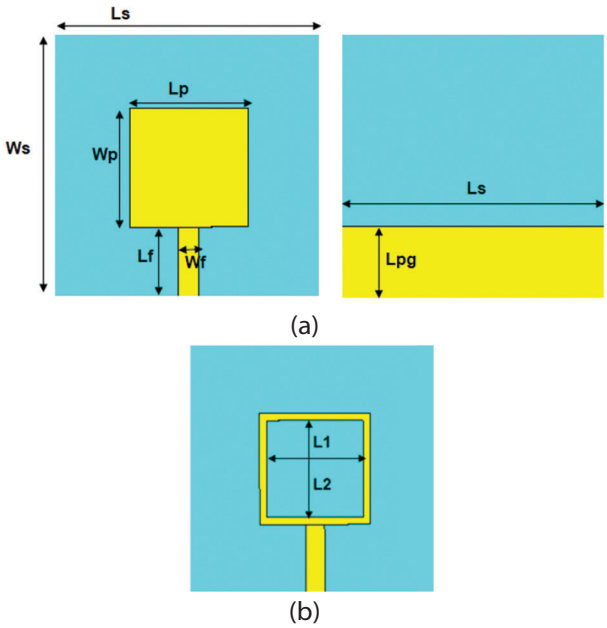

Fig. 1. (a) Front and ground view (b) Modified slot patch

The simulated response of the return loss and axial ratio for both shapes are presented in Fig. 2. Fig. 2(a) clearly shows that the slot square effects the return loss by shifting the frequency to the lower bands compared to the standard MPA. In Fig. 2(b), the axial ratio is above the required 3 dB level at 3.5 GHz for both antennas. Secondly, four square fractal shapes connected as a plus topology are added to the modified slot patch.

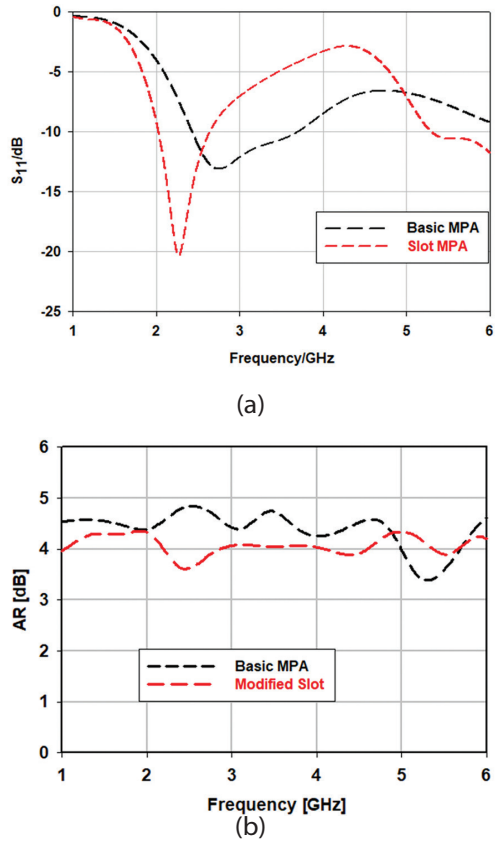

Fig. 2. Parametric study, (a) Return loss, (b) Axial ratio

The following equation is used to calculate the length of the first iteration of the square:

$$L_i = L_{i-1} * S \quad (1)$$

where the iteration is i = 1, 2, 3, 4,..., and S is the scaling factor reducing the size. Fig. 3 shows the proposed fractal antenna design process. The proposed fractal shape is inserted into the slot square shape as a matrix fractal of 3 × 4, where the fractal matrix is connected in the upper line of the modified square antenna, as observed in Fig. 3(a). In order to increase the impedance bandwidth and return loss, a U-shaped slot is added in the feed line, as in Fig. 3 (a). This helps the suggested antenna cover more spectrum and enhance the matching impedance.

Finally, as shown in Fig. 3(b), a fractal shape is added to the top corner of the proposed antenna to increase bandwidth and improve AR. The modified shapes with two flower shapes added to the antenna's left corner, followed by the same shapes added to the right corner as in Fig. 3 (b), with the same partial ground plane. Fig. 4 shows the parametric study on return loss and axial ratio as a better enhancement is achieved for both responses. Finally, the partial ground is modified with two rectangular slots cut distributed on both left and right sides of the feed line. Also, a T-shape slot cut is made on the partial ground to broaden the bandwidth and enhance the return loss order to cover more sub-6 GHz bands as illustrated in Fig. 5. The final dimensions for the suggested fractal antenna with amended ground plane are presented in Table 1.

Table 1. The final dimension for the modified ground fractal antenna

Parameters	Value (mm)	Parameters	Value (mm)
Ls	50	Lsq^2	1.75
Ws	50	Lsq^3	0.8
Lp	27.4	*R1*	4.7
Wp	27.4	*R2*	2.04
Lf	21	*Lf1*	58.8
Wf	5.3	*Lf2*	25.6
Lpg	70	*Lc1*	8
L1	25.2	*Lc2*	5.6
L2	25.2	*Ls1*	7
R1	1.5	*R2*	0.75
Lsq	3.5	Sub-6 GHz	
Slot dimension		4 × 0.56 mm²	

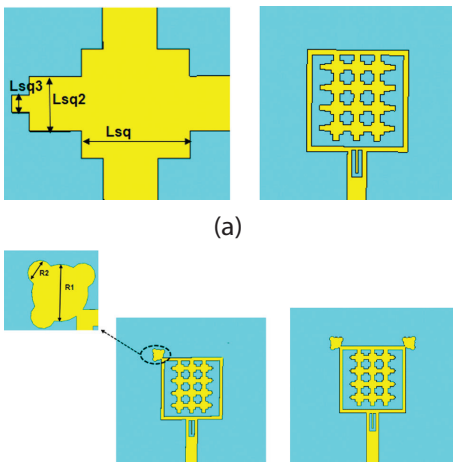

(a)

(b)

Fig. 3. (a) Fractal square proposed for fractal antenna. (b) The modified antenna with flower shape fractal added to the corner of the fractal MPA

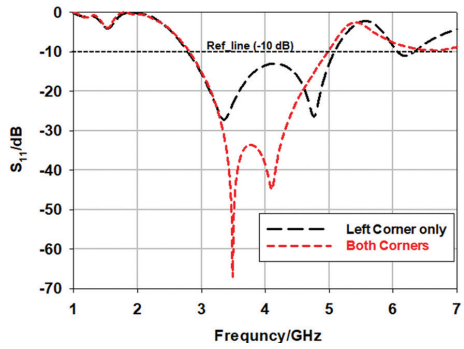

(a)

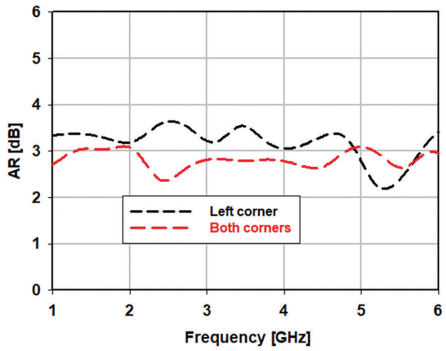

(b)

Fig. 4. Parametric study by adding fractal and flower shape, (a) Return loss enhancement, (b) Axial ratio enhancement

Fig. 6 shows the performance of the optimized fractal MPA with modified partial ground in terms of return loss (S_{11}), radiation pattern, gain, and axial ratio (AR). At 4.2 GHz, a maximum return loss of -46 dB is achieved, resulting in an impedance bandwidth of 4 GHz. As shown in Fig. 6 (a), A return loss of below -10 dB is obtained over the whole bandwidth. A radiation pattern at a specific frequency of 4 GHz is plotted in Fig. 6 (b). 3.62 dB of directivity is reported. Fig. 6 (c) illustrates the gain value over the obtained bandwidth that ranges from 1.8 dB to 5.6 dB, with a 1.8 minimum value gain and a 5.6 maximum value gain at 1.8 GHz and 5.8 GHz, respectively. According to Fig. 6(d), an excellent circular polarization is indicated by the fact that the axial ratio is below 3 dB throughout the whole bandwidth.

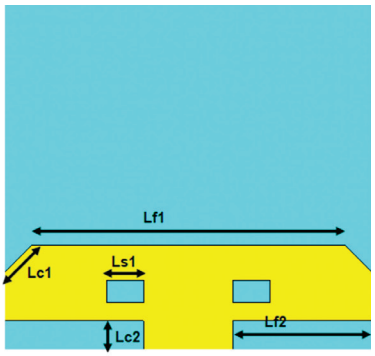

Fig. 5. Modified slot of Partial ground plane

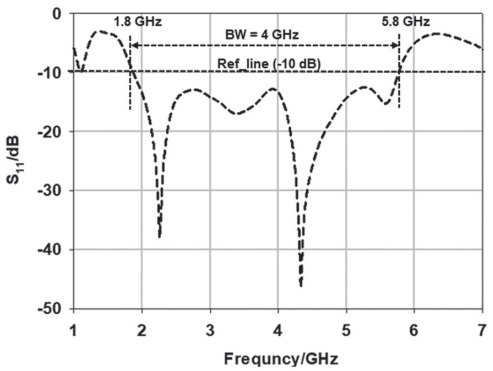

(a)

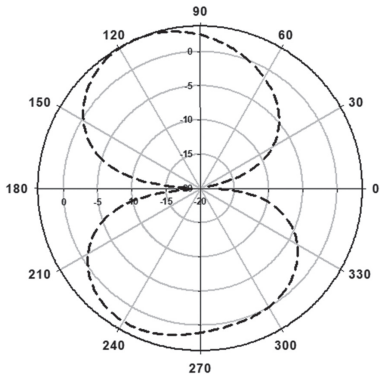

(b)

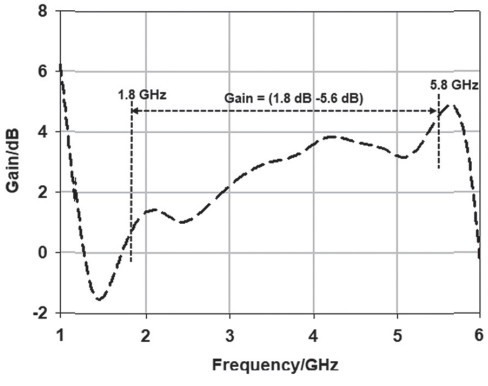

(c)

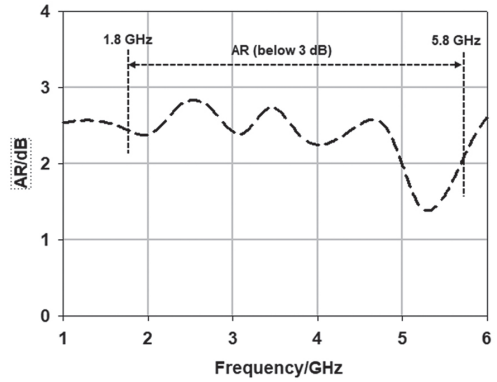

(d)

Fig. 6. The performance of the suggested fractal antenna with modified partial ground plane. (a) Return loss. (b) Radiation pattern. (c) Gain. (d) AR.

2.2. DESIGN OF METASURFACE WITH ANTENNA

Resonant frequency (f) is a property of metasurface. Calculating the resonant frequency takes into account the transmission line's capacitance (C) and inductance (L) properties. The frequency can be changed to a higher or lower frequency or in the direction of the desired frequency by adjusting the capacitance and inductance values. Generally, metasurface resonant frequency (f) is determined theoretically by its inductance (L) and capacitance (C). The resonant frequency varies by changing the values of inductance and capacitance The resonant frequency can be determined by [13]:

$$f = \frac{1}{2\pi\sqrt{LC}} \tag{2}$$

A dielectric substrate has a lattice etched into it to filter the element's conductivity. This creates a complete metasurface made up of several unit cells. Additionally, it enables the metasurface to pass or reject particular signals at a particular frequency. Therefore, in order to maximize the antenna's gain and bandwidth, a metasurface is created using a square split ring resonator (SSRR).

Four SSRR cells compose the unit cell, as seen in Fig. 7. The four SSRR's frequency is determined by [26]:

$$f_0 = \frac{1}{2\pi\sqrt{L\left[\left(2l-\frac{g}{2}\right)C+\frac{\varepsilon_0 wh}{2g}\right]}} \tag{3}$$

The final resonator width is (SS), and the cut in each SSR is (g). The capacitance and the inductance can be determined as:

$$C = \frac{\sqrt{\varepsilon_e}}{c_0 Z_0} \tag{4}$$

$$L = 0.00508l\left(2.303\log_{10}\frac{4l}{w} - \theta\right) \tag{5}$$

$$l = \frac{\lambda}{N} \quad \text{N= 4, 10, 20, …., N-1} \tag{6}$$

Hence, the values of the unit cell are as follows: (L=7mm, WW=0.5mm, S=0.4 mm, g=0.5mm, and SS=1 mm). Fig. 8 displays the performance of the SSRR unit cell in terms of S-parameters, permittivity (ε), and permeability (μ).

Metamaterials can be epsilon negative materials (ENG), mu negative materials (MNG), or double negative materials (DNG) [27]. Adding a number of SSRR's array (SSRR, SSRR2, SSRR3) to the form shifts the return loss (S11) below 3.5 GHz, as illustrated in Fig. 8 (a). The transmission coefficient lags behind the return loss at a lower frequency, as shown in Fig. 8(b), when compared to a higher frequency greater than 3.5 GHz. At sub-6 GHz the permeability is positive, While the permittivity is negative between 3 and 4 GHz as depicted in Fig. 8 (c) and Fig. 8 (d), respectively. As a result, the suggested metamaterial unit cell elements used in this paper, namely SSRR (the simplest realization of an LC circuit as a metamaterial element) acts as an ENG.

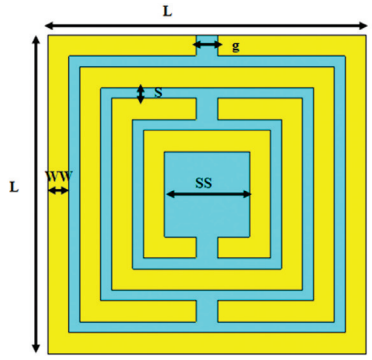

Fig. 7. SSRR unit cell design

Hence, metasurface is filtered by consisting of lattice of elements conductivity etched on a substrate dielectric. That allows metasurface unit cells to configure for selective frequencies to reject and pass through signals of certain frequency. As a result, the SSRR unit cell is integrated to create a 5 × 5 metasurface configuration, as seen in Fig. 9. Due to the suggested metasurface's symmetry, the cross-polarization and co-polarization of the normal x-polarized EM wave will be identical. Co-polarization between 4.2 GHz and 4.45 GHz is less than -10 dB. As shown in Fig. 10 (a), co-polarization is still less than -10 dB at frequency ranges over 6 GHz. The cross-polarization value in the mid-band (at 3.5 GHz) is within -1 dB. The Perfect conductor resonator (PCR) achieved a value more than 90% at 3.5 GHz and 5.8 GHz, as in Fig. 10 (b). As a result, the metasurface confirms the current surface increase in order to improve the gain.

To verify the high gain property shown in Fig. 11, A recommended fractal antenna is positioned above the suggested 5 × 5 metasurface. In the proposed configuration, a metasurface layer with unit cells faces the antenna from above and is separated from the bottom fractal antenna layer by an air separation gap between the layers (d).

The comparison of the simulated findings for the antenna's return loss, gain, axial ratio, and radiation pattern with respect to the metasurface at d = 15 mm is seen in Fig. 12. The return loss for both antennas with metasurface at 3.5 GHz is found to be -23.5 dB with a

fractional bandwidth of 3 GHz, as depicted in Fig. 12 (a). Fig. 12 (b) shows that the gain increases to 7.33 dB when the SSRR metasurface is used, which is comparable to the fractal antenna's gain of 2.33 dB. In both cases, the axial ratios remained constant along the bandwidth with a value below 3 dB, as illustrated in Fig. 12(c). Without the application of a metasurface, a circularly polarised radiation pattern can be observed compared to a directed radiation pattern when a metasurface is employed, as in Fig. 12 (d). Hence, the antenna with the metasurface demonstrated excellent impedance bandwidth, high gain, and a wide axial ratio in the simulation. The antenna measurement outcomes with the metasurface utilized will be discussed in the next section.

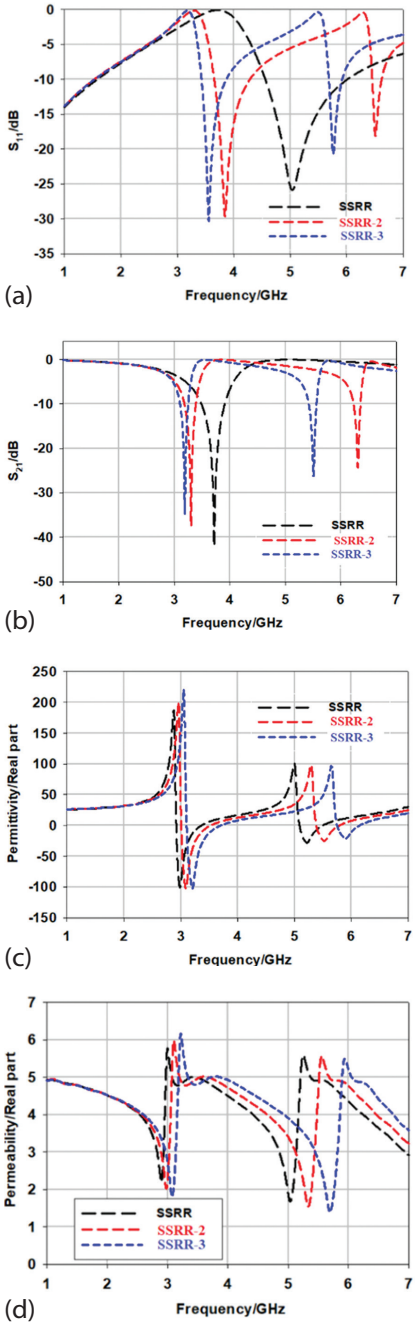

Fig. 8. Performance of the SSRR unit cell. (a) Return loss. (b) Transmission. (c) Permittivity. (d) Permeability

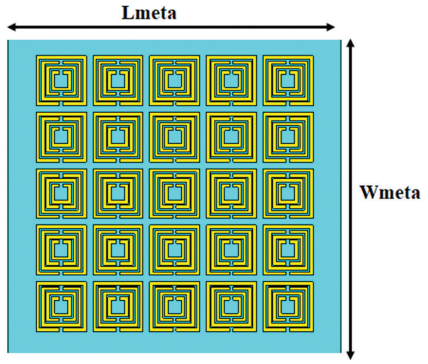

Fig. 9. The suggested configuration of 5 × 5 metasurface

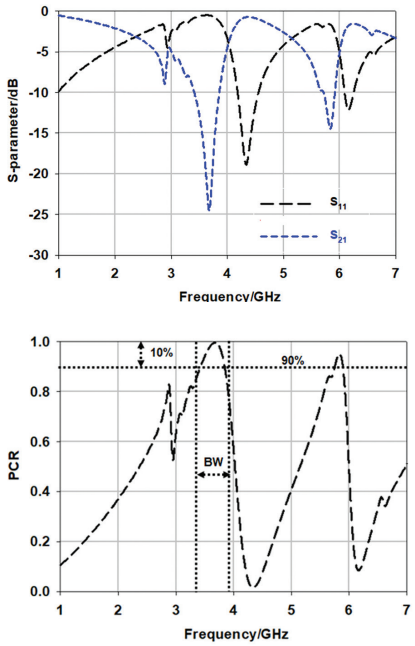

Fig. 10. Simulated response of 5 × 5 metasurface (a) return loss and transmission, (b) PCR

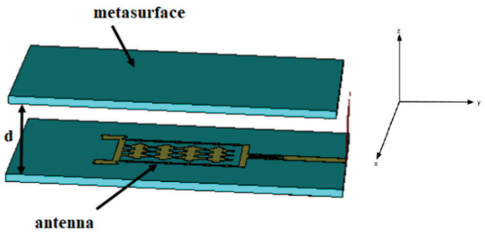

Fig. 11. The suggested metasurface positioned above the antenna

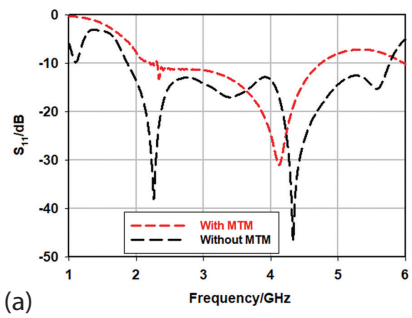

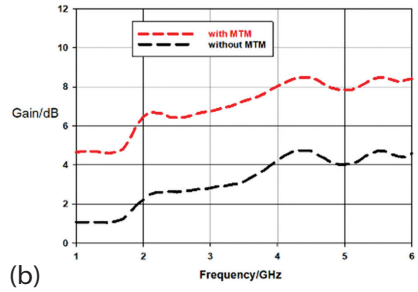

(b)

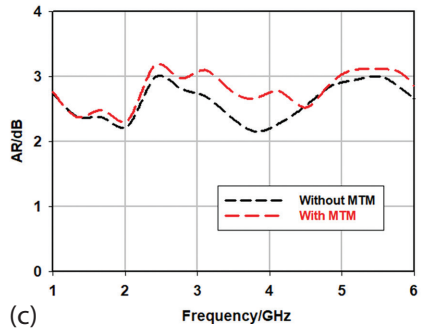

(c)

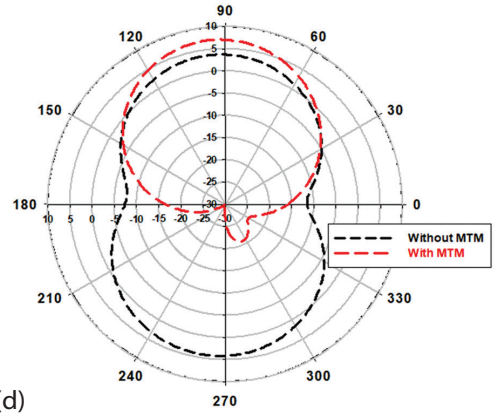

(d)

Fig. 12. Comparison of suggested antenna with and without Metasurface. (a) Return loss. (b) Axial ratio. (c) Radiation pattern. (d) Gain

3. RESULTS AND DISCUSSION

In this section fabrication and measurement results of fractal and metasurface antenna are introduced and compared with simulated results.

3.1. ANTENNA RESULTS

The printed fractal antenna in Fig. 13 is depicted with dimensions of 50 mm × 50 mm highlighting the compact size of the fractal antenna. Using the Keysight (Agilent Technologies) N9925A vector network analyser (VNA), the measurement in terms of S-parameters is carried out. Fig. 14 compares the printed fractal antenna's performance to simulation findings in terms of return loss, radiation pattern, gain, and AR. Fig. 14 (a) displays the printed antenna's measured return loss. Compared to the simulated result, the fractal antenna has a return loss of -12.45 dB at 3.5 GHz with a bandwidth of 3.16 GHz. The suggested antenna's simulated and measured radiation patterns in both directions are shown in Fig. 14(b).

In comparison to the simulated one, the measured prototype's major lobe is seen to be tilted by 3 degrees. According to the measurements, the prototype's sidelobes are slightly low. The measured and simulated realized gain for the proposed antennas is plotted in Fig. 14 (c). In comparison to the simulated gain of 3.05 dB, the measured gain at 3.5 GHz is 2.61 dB, indicating a slight loss of 0.5 dB. The primary cause of the decrease is the unwanted interference from the surrounding environment.

The plot of the measured and simulated antenna AR over frequency is observed in Fig. 14(d). The measured AR of the proposed antennas is well above 80% within the operating frequency. The measured AR is 2.9 dB at 3.5 GHz. Due to high radiation efficiency, the gap between the measured and simulated AR is slightly smaller in the 1.79 GHz to 5 GHz bandwidth range.

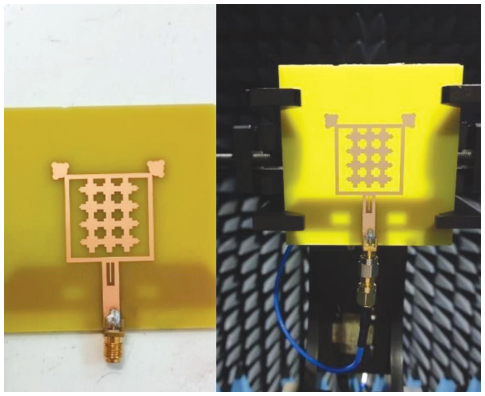

(a)

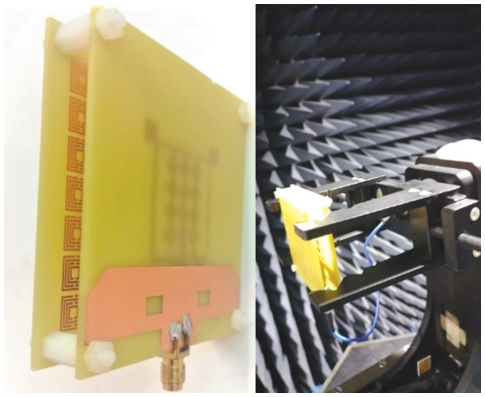

(b)

Fig. 13. The printed prototypes. (a) fractal antenna, (b) metasurface antenna

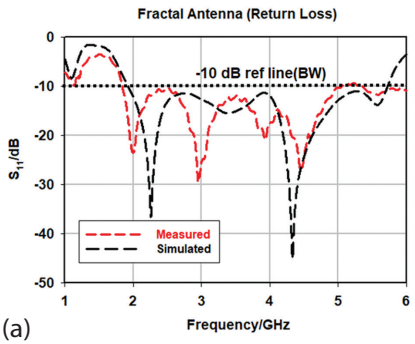

(a)

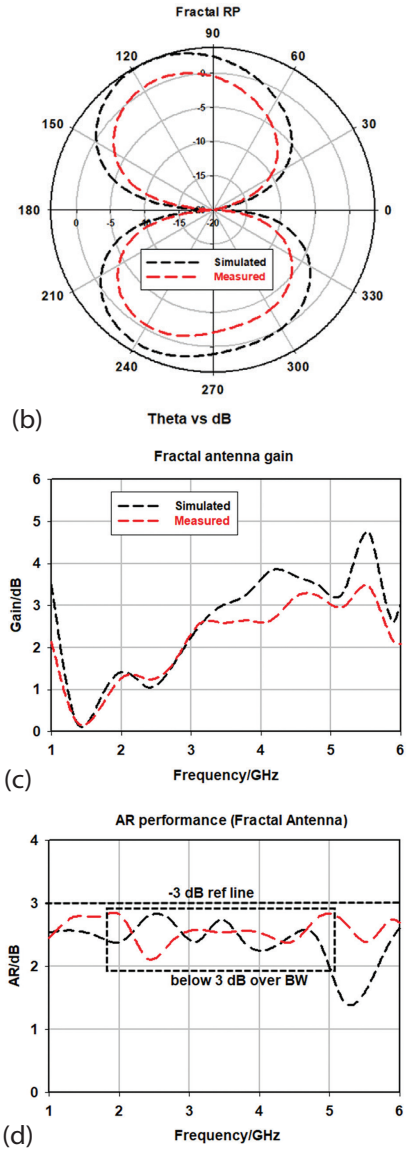

Fig. 14. The measured performance of the printed fractal antenna: (a) Return loss, (b) Radiation pattern, (c) Gain, (d) AR

3.2. METASURFACE ANTENNA RESULTS

Fig. 15 (a) displays the measured return loss performance. At 4 GHz, the measured S11 is -23.58 dB versus a simulated value of -30.2 dB. With a loss of 100 MHz of simulated bandwidth (3 GHz), the measured fractional bandwidth is 2.99 GHz. As seen in Fig. 15 (b), the measured radiation pattern and the simulated one agree well with a 3-degree erroneous tilt. The observed gain response is contrasted with the simulated one in Fig. 15 (c). The measured gain, in comparison to the simulated 8 dB gain, is 7.2 dB with a loss of 0.8 dB. This is due to interfering sources within the radiation pattern chamber. In Fig. 15 (d), the AR performance is compared. The AR value is greater than 82% over the operational frequencies. For instance, at 4 GHz, there is only a 0.5 dB difference between the measured and simulated AR. Table 2 compare the measured results of metsurface antenna with the simulated ones. Table 3 includes a comparison between different metamaterial-based circularly polarized antennas.

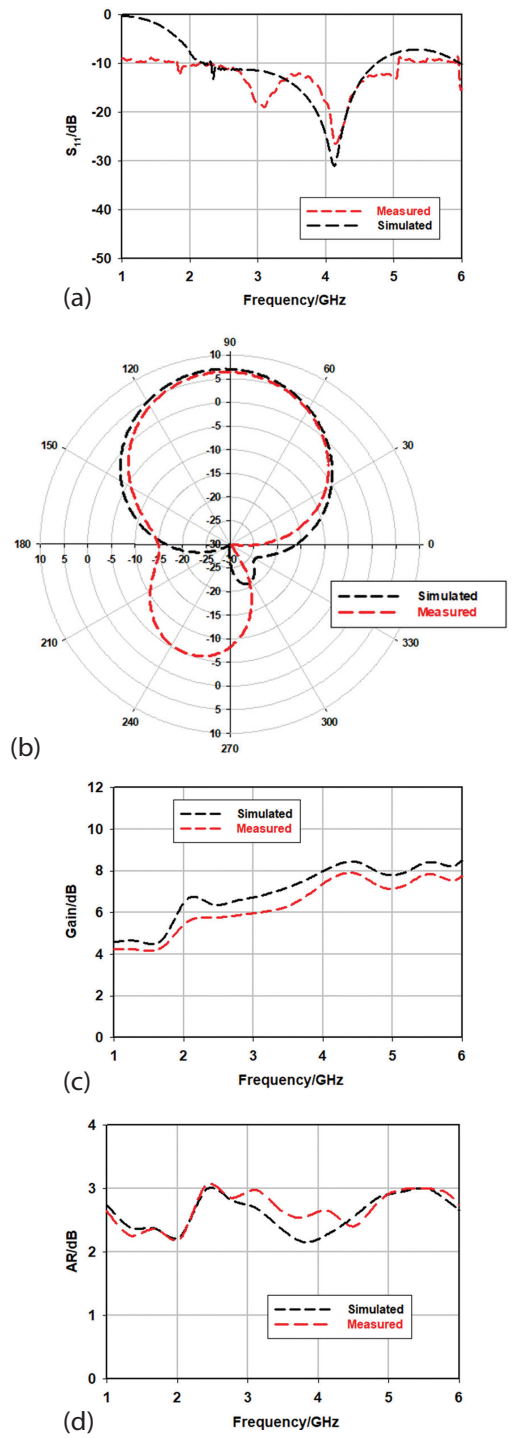

Fig. 15. Performance of the measured printed metasurface antenna: (a) Return loss, (b) Radiation pattern, (c) Gain, (d) AR

Table 2. comparison between the measured results of metsurface antenna with the simulated ones

Parameters/metasurface	Simulated	Measured
Return loss (S11)	-15.25	-12.45
Bandwidth (GHz)	3.8	3.16
Gain (dB)	3.05	2.61
AR (dB)	2.7	2.9

Table 3. Comparison between different metamaterial-based circularly polarized antennas

Comparison with related works					
Ant	**Feeding method &resonant freq**	**Gain dBic**	**Impedance bandwidth**	**AR band**	**Observations And complexity**
[28]	Coaxial probe feed 3 GHz	4.15	2.92-3.06 GHz	3.11-3.17 GHz	Crossbar fractal tree slot and three-turn complementary spiral resonators
[29]	CPW feed 1.95 &2.61 GHz	6.9 1.1	1.94 t-1.965 GHz 2.545-2.685 GHz	2.60 - 2.62 GHz	(CRLH)composite right/left-handed unit cell is designed as a radiation element
[30]	Coaxial probe feed Around 3 GHz	0.4-0.95	1.475-1.483 GHz 1.481-1.489 GHz	1.479-1.486 GHz	Structure is quite complicated; the gain is also quite low
[31]	Coaxial probe feed Around 3 GHz	6.26 6.97	2.875-2.961 GHz 3.812-3.836 GHz	2.879-2.901 GHz 3.822-3.829 GHz	Provides a very narrow operational bandwidth
This work	Microstrip feed 3.5 GHz	6	1.79 – 5 GHz	1.82-5 GHz	Simple method using square fractal shapes and flower fractals

4. CONCLUSION

This study discusses a 3.5 GHz wideband circularly polarized fractal antenna, the square and flower fractal shapes were used to create the fractal antenna. Then metamaterials structures are developed as metasurface to increase the gain and reduce the side lobes of the proposed antennas. The metamaterial designed individually at the same frequency type and is selected based on the current works on enhancement specifically parameters such as size, bandwidth, and gain. The performance of the proposed design validated through measurement process and it was much in line with the simulation's findings. The designed antenna achieved great S-parameters, bandwidth, and AR performance. A high fractional bandwidth of 91% is provided by the antenna which operates in the 1.79 GHz to 5 GHz frequency range. By 40.43%, the antenna had successfully acquired a favorable profile of compact size. The suggested antenna is appropriate for use in a future antenna array system for 5G.

5. REFERENCES:

[1] Y. He, S. Lv, L. Zhao, G.-L. Huang, X. Chen, W. Lin, "A compact dual-band and dual-polarized millimeter-wave beam scanning antenna array for 5G mobile terminals", IEEE Access, Vol. 9, 2021, pp. 109042-109052.

[2] I. Syrytsin, S. Zhang, G. F. Pedersen, A. S. Morris, "Compact quad-mode planar phased array with wideband for 5G mobile terminals", IEEE Transactions on Antennas and Propagation, Vol. 66, No. 9, 2018, pp. 4648-4657.

[3] N. O. Parchin, J. Zhang, R. A. Abd-Alhameed, G. F. Pedersen, S. Zhang, "A planar dual-polarized phased array with broad bandwidth and quasi-endfire radiation for 5G mobile handsets", IEEE Transactions on Antennas and Propagation, Vol. 69, No. 10, 2021, pp. 6410-6419.

[4] Y. Kumar, S. Singh, "Microstrip Fed Multiband Hybrid Fractal Antenna for Wireless Applications", Applied Computational Electromagnetics Society Journal, Vol. 31, No. 3, 2016, pp. 327-332.

[5] M. I. Sabran, S. K. A. Rahim, P. J. Soh, C. Y. Leow, G. A. E. Vandenbosch, "A Simple Electromagnetically Fed Circularly Polarized Circular Microstrip Antenna", Applied Computational Electromagnetics Society Journal, Vol. 30, No. 11, 2015, pp. 1180-1187.

[6] M. Majidzadeh, J. Nourinia, C. Ghobadi, "Compact CPW-Fed Antenna with Circular Polarization Characteristics in WLAN Frequency Band", Applied Computational Electromagnetics Society Journal, Vol. 28, No. 10, 2013, pp. 938-943.

[7] Y. Liu et al. "A K-band broadband circularly polarized slot antenna based on L-shaped waveguide cavity", IEEE Antennas and Wireless Propagation Letters, Vol. 20, No. 9, 2021, pp. 1606-1610.

[8] Z. Zhou, Z. Wei, Z. Tang, Y. Yin, "Design and analysis of a wideband multiple-microstrip dipole antenna with high isolation", IEEE Antennas and Wireless Propagation Letters, Vol. 18, No. 4, 2019, pp. 722-726.

[9] X. Shuai, S. Xiao, "A novel dual-band circularly polarized slot antenna with fractal slot geometry: Shuai and Xiao", Microwave and Optical Technology Letters, Vol. 59, No. 2, 2017, pp. 451-456.

[10] S. Maity, K. R. Barman, S. Bhattacharjee, "Silicon-based technology: Circularly polarized microstrip patch antenna at ISM band with miniature structure using fractal geometry for biomedical application", Microwave and Optical Technology Letters, Vol. 60, No. 1, 2018, pp. 93-101.

[11] K. S. Kola, A. Chatterjee, D. G. Patanvariya, "Design of a wideband right-handed circularly polarized ar-

ray of miniaturized mushroom-shaped antennas for direct broadcast satellite application", Microwave and Optical Technology Letters, Vol. 62, No. 11, 2020, pp. 3542-3555.

[12] E. Wang, M. Liu, D. Lin, J. Wang, "A compact circular polarized patch fractal antenna for global navigation satellite systems", Microwave and Optical Technology Letters, Vol. 64, No. 3, 2022, pp. 520 – 524.

[13] H. A. Atallah, A. B. Abdel-rahman, K. Yoshitomi, R. K. Pokharel, "Mutual Coupling Reduction in MIMO Patch Antenna Array Using Complementary Split Ring Resonators Defected Ground Structure", Applied Computational Electromagnetics Society Journal, Vol. 31, No. 7, 2016, pp. 737-743.

[14] G. Mansour, E. Nugoolcharoenlap, R. H. Mahmud, T. Tippo, P. Akkaraekthalin, D. Torrungrueng, "Circularly Polarized Elliptical Patch Array Antennas for GPS", Proceedings of the Research, Invention, and Innovation Congress, Bangkok, Thailand, 1-3 September 2021.

[15] M. Asad Rahman, E. Nishiyama, I. Toyoda, "A Circular Polarization Antenna with Square Ring Slot Loaded on Ground Plane", Proceedings of the International Symposium on Antennas and Propagation, Phuket, Thailand, 30 October - 2 November 2017.

[16] A. Sihvola, "Metamaterials in electromagnetics", Metamaterials, Vol. 1, No. 1, 2007, pp. 2-11.

[17] J. Undrakonda, R. K. Upadhyayula, "A Novel Miniaturized Isotropic Patch Antenna for X -Band Radar Applications Using Split Ring Resonators", International Journal of Electrical and Computer Engineering Systems, Vol. 14, No. 1, 2023, pp. 21-27.

[18] C. R. Simovski, "Material Parameters of Metamaterials (a Review)", Optics and Spectroscopy, Vol. 107, No. 5, 2009, pp. 726-753.

[19] A. K. Vallappil, B. A. Khawaja, M. K. A. Rahim, M. N. Iqbal, H. T. Chattha, "Metamaterial-Inspired Electrically Compact Triangular Antennas Loaded with CSRR and 3 × 3 Cross-Slots for 5G Indoor Distributed Antenna Systems", Micromachines, Vol. 13, No. 2, 2022.

[20] K. Jairath, N. Singh, M. Shabaz, V. Jagota, B. Kumar Singh, "Performance Analysis of Metamaterial-Inspired Structure Loaded Antennas for Narrow Range Wireless Communication", Scientific Programming, Vol. 2022, 2022.

[21] F. H. Lin, Z. N. Chen, "Low-profile wideband metasurface antennas characteristics mode analysis", IEEE Transactions on Antennas and Propagation, Vol. 65, No. 4, 2017.

[22] Z. Liang, J. Ouyang, F. Yang, "Low-profile wideband circularly polarized single-layer metasurface antenna", Electronics Letters, 2018, Vol. 54, No. 24, 2018, pp. 1362-1364.

[23] W. Lin, Z. N. Chen, X. Qing, "Metamaterial-based low profile broadband mushroom antenna", IEEE Transactions on Antennas and Propagation, Vol. 62, No. 3, 2014, pp. 1165-1172.

[24] Q. Chen, H. Zhang, "Dual-patch polarization conversion metasurface-based wideband circular polarization slot antenna", IEEE Access, Vol. 6, 2018, pp. 74772-74777.

[25] T. Tu Le, H. H. Tran, A. A. Althuwayb, "Wideband Circularly Polarized Antenna Based on a Non-Uniform Metasurface", Applied Science, Vol. 10, No .23, 2020.

[26] Y. Dong, T. Itoh, "Metamaterial-Based Antennas", Proceedings of the IEEE, Vol. 100, No. 7, 2012.

[27] G. V. Eleftheriades, K. G. Balmain, "Negative-refraction metamaterials: fundamental principles and applications", John Wiley & Sons, 2005.

[28] H.-X. Xu, G.-M. Wang, J.-G. Liang, M. Q. Qi, X. Gao, "Compact Circularly Polarized Antennas Combining Meta-Surfaces and Strong Space-Filling Meta-Resonators", IEEE Transactions on Antennas and Propagation, Vol. 61, No. 7, 2013, pp. 3442-3450.

[29] C. Zhou, G. Wang, Y. Wang, B. Zong, J. Ma, "CPW-Fed Dual-Band Linearly and Circularly Polarized Antenna Employing Novel Composite Right/Left-Handed Transmission-Line", IEEE Antennas and Wireless Propagation Letters, Vol. 12, 2013, pp. 1073-1076.

[30] B.-C. Park, J.-H. Lee, "Omnidirectional Circularly Polarized Antenna Utilizing Zeroth-Order Resonance of Epsilon Negative Transmission Line", IEEE Transactions on Antennas and Propagation, Vol. 59, No. 7, 2011, pp. 2717-2721.

[31] S.-T. Ko, B.-C. Park, J.-H. Lee, "Dual-Band Circularly Polarized Patch Antenna with First Positive and Negative Modes", IEEE Antennas and Wireless Propagation Letters, Vol. 12, 2013, pp. 1165-1168.